



Significant fluorescence intensity of excitation dependent emission at longer wavelength of graphite-ZnO nanocomposite in water: A cyanide sensor

Tanmoy Ghosh^a, Soumyadeep Mitra^a, Suman Kumar Maity^{a,b}, Somrita Mondal^{*a} and Dilip K. Maiti^{*a}

^aDepartment of Chemistry, University College of Science, 92, Acharya Prafulla Chandra Road, Kolkata-700 009, India

^bDepartment of Chemistry, Narasinha Dutt College, University of Calcutta, 129, Belilious Road, Howrah-711 101, West Bengal, India

E-mail: dkmchem@caluniv.ac.in

Manuscript received online 12 October 2020, revised and accepted 27 November 2020

During the last few years, carbon-based nanomaterials have been widespread topic of research due to their easy access from plentiful raw materials, scalable and facile synthesis procedures, high chemical stability, resilient to photo-bleaching, low toxicity, and susceptible to chemical modification. Carbon-based nanomaterials exhibit another exciting property – the excitation dependent fluorescence emission. This unique property has significant applications in sensing, imaging, solar cell and photovoltaics. Nevertheless, applications using the exceptional excitation dependent fluorescence property of carbon-based nanomaterials has not been investigated so far because most of the reported excitation-dependent emission of carbon-based nanomaterials cause a substantial decrease in fluorescence intensity value, especially at the longer wavelength region. In this article, we report simple aqueous syntheses of ZnO-graphite nanocomposites utilizing inexpensive and readily available Zn(OAc)₂·2H₂O and graphite. The as-synthesized nanocomposites display unusual excitation-dependent fluorescence emission without noteworthy drop in fluorescence intensity value, specifically at the longer wavelength region. Furthermore, the intensity of fluorescence of the ZnO-graphite nanohybrids consistently enhanced with addition of micromolar cyanide ion. The augmentation of fluorescence of nanocomposites in presence of cyanide fitted well in Langmuir binding isotherm. This fitting allows sensing of cyanide in quantitative way. This exclusive excitation-dependent fluorescence emission property of the ZnO-graphite nanocomposite along with the phenomenon of augmentation in fluorescence intensity of the nanocomposite with addition of cyanide ion pave the way for fabrication of a array-based chemical nose sensor for detection of environmentally toxic anions similar to cyanide.

Keywords: Excitation dependent fluorescence emission, ZnO-graphite nanocomposites, emission at longer wavelength, Langmuir binding isotherm, cyanide sensing.

Introduction

In recent years, excitation reliant photoluminescence¹⁻⁴, phenomena exhibited by the family of carbon-based nanomaterials, has received substantial attention. Several pioneering examples, including graphene⁴⁻⁶, graphite^{7,8}, diamonds^{9,10}, carbon nanotubes^{4,11}, fullerenes^{12,13}, carbon dots¹⁴⁻²⁶ and combustion candle soot²⁷ have recently been reported in the literature^{28,29}.

In spite of having variance in size, shape, and surface, most of the carbon-based nanomaterials reveal analogous excitation dependent fluorescence behavior in the visible region^{23,30,31}. Usually, a bathochromic shift is observed for increasing in excitation wavelength of the emission of car-

bon nanomaterials³². The carbon-based nanomaterials are easy to furnish from readily available raw materials^{33,34}, and their synthetic procedures are scalable with little environmental audaciousness^{8,27,35}. Moreover, these materials have good solubility⁸, excellent chemical stability¹¹, resilient to photo-bleaching¹¹, low toxicity³⁴, and susceptible to chemical modification^{9,36}. Owing to these privilege, carbon-based nanomaterials have been extensively used for many prospective applications⁴ including bio-sensing³⁷, catalysis¹⁷, biomedicine³⁸, bioimaging^{11,39} and optoelectronic devices⁴⁰. Despite several opportunities, the application using the unique excitation-reliant fluorescence emission of carbon-based nanomaterials is very limited. One of the primary reasons for

this drawback is the fact that the bathochromic shift of the fluorescence emission is escorted with an enormous decrease of fluorescence intensity in the longer wavelength region. For instance, excitation-dependent emission of graphene oxide nanosheets^{41–43}, carbogenic nanoparticles⁴⁴, carbon nanoparticles⁴⁵, and carbon nanodots⁴⁶ displayed excitation dependent emission i.e. shifting of fluorescence emission maxima with the increasing of excitation wavelength, but the excitation dependent fluorescence intensity dropped miserably in the longer wavelength region, as reported in the literature^{41–46}. Therefore, the fluorescence property cannot be truly termed as excitation-dependent phenomena. Thus, there is in dire need of engineering excitation-dependent fluorescence emission without a noteworthy drop in fluorescence intensity, so that the excitation dependent fluorescence property can be utilized for several applications.

Among all semiconductor transition metal oxides, ZnO is one of the most popular material for sensing applications owing to several advantages e.g. wide band gap, high chemical and thermal stability, low toxicity, appreciable oxidation potential, large exciton binding energy^{47,48}. ZnO nanostructures and nanocomposites have quite interesting optical properties. A simple variation in the synthetic route to fabricate ZnO nanocomposites with different size, shape, electron density can give rise to unique optoelectronic properties⁴⁹ leading to potential applications in the arena of biomedicine, sensors and development of optical instrumentation components⁵⁰. Among these unique properties, fluorescence is one of the most notable features for modified ZnO nanostructures and composites. Modified fluorescence can strengthen some of their characteristics and endorse innovative properties⁵¹ for several applications e.g. transparent photoelectrodes⁵², sensors⁵³, solar cell circuits⁵⁴. For instance, addition of Cr nanoclusters in ZnO films has been reported to exhibit a strong optical Kerr effect. The enormous fluorescence response and refractive nonlinearity of the photoconductive modified zinc oxide samples have prospective applications for progress of multifunctional all-optical nanodevices⁵⁵. Similarly, a noteworthy nonzero nonlinear optical response was reported for Li doped ZnO nanorods. The sample showed stimulated emission and third order optical nonlinearity⁴⁹. The stimulating lasing response of this doped ZnO can be improved by change in alignment, harvesting better optical cav-

ity. Thus, interesting optical properties arising in modified zinc oxide nanoparticles and nanocomposites seem to be appealing as they give rise to unexpected physical properties. Moreover, graphene oxide-ZnO nanocomposites have showed effective applications in sensing for sensing hydrogen sulphide (H₂S)⁵⁶, CO, NH₃, NO NO₂, H₂, CH₄⁵⁷, 8-hydroxy-2'-deoxyguanosine⁵⁸, Levodopa, Tyrosine etc.⁵⁹. Considering the aforesaid advantages of ZnO as well as composite of ZnO as sensor, incorporation of ZnO nanostructures within graphite nanosheets for application in sensing can be interesting.

Herein, we demonstrate the simple, aqueous, and scalable synthesis of graphite-ZnO nanocomposite. The as-synthesized nanocomposite displays appealing excitation dependent fluorescence emission in the visible region, covering a broad range of 400–500 nm. In our case, excitation dependent emission occurs without substantial drop in fluorescence intensity, especially at the longer wavelength region. Further, upon excitation at 340 nm, the fluorescence emission intensity of the ZnO-graphite nanocomposite drastically enhances with the addition of millimolar cyanide ion. Thus, we communicate herein our preliminary results for applicability of the phenomena to sense toxic anion like cyanide as an example. This can pave the way to design a multichannel array-based sensor for detection of toxic anions present in the drinking water, industrial wastes, and other sensitive aqueous effluents.

Experimental details

Synthesis of ZnO nanowires and nanoflowers:

ZnO Nanowire was synthesized following sol-gel method (Scheme S1, Supporting Information)^{60,61}. Zn(OAc)₂·2H₂O (2 mg, 0.011 mmol) was solubilized in water (10 mL) and stirred for 1 h under mild heating conditions. Aqueous NaOH (0.0125 N, 10 mL) was added to the aforementioned reaction mixture and stirred vigorously for 30 min. Next, the solution was kept in a beaker and drop-wise methanol (125 mL) was added to it with continuous stirring. A milky white precipitate appeared and the reaction content was allowed to precipitate out the nanoparticles (NPs) completely in 15 h. The nanoparticles were filtered, followed by washing with water for several times and kept in a vacuum oven. Finally, the powdered ZnO-white nanomaterials were collected and stored.

Synthesis of ZnO-graphite nanocomposite (Method 1):

The as-synthesized ZnO powder (2 mg) was dispersed in water (5 mL) and sonicated for half an hour (Scheme S2, Supporting Information). Graphite powder (5 mg) was dissolved in water (5 mL) and sonicated. The black graphite solution was added drop-wise to the ZnO suspension in water. The solution was centrifuged and washed water several times. The suspension was further dissolved in water (10 mL). Further, the solution was autoclaved at 140°C for 20 h. The resultant solution was centrifuged and washed with ethanol and acetone. It was kept in a vacuum oven for overnight. Finally, the grey color powdery graphite:ZnO::1:1 nanocomposite was collected and stored. The similar procedure was repeated with ZnO:graphite ratio 2:1 (4 mg and 5 mg respectively) to synthesize ZnO:graphite::2:1 nanocomposite.

Synthesis of ZnO-graphite nanocomposite (Method 2):

Zn(OAc)₂·2H₂O (4 mg, 0.022 mmol) and graphite (5 mg) were sonicated in water (20 mL) for 1 h. Next, aqueous NaOH (0.0125 N, 20 mL) was added to the previous solution and the reaction mixture was sonicated for 30 min. Ethanol (80 mL) was added dropwise with continuous stirring, and the resulting solution was sonicated (30 min). Further, the solution mixture was kept in an autoclave at 160°C for 20 h. Finally, the dry powder was collected in which the ZnO nanoflowers were grown on graphite sheet *in situ*.

Results and discussion

Synthesis of the nanocomposites:

First, ZnO nanowires were fabricated using Zn(OAc)₂·2H₂O following sol-gel method^{60,61} under alkaline conditions (Scheme S1, Supporting Information). Syntheses of graphite-ZnO nanocomposites were performed through mixing as-synthesized ZnO nanomaterials and graphite powder in water medium (Scheme S2, Supporting Information) followed by thermal treatment in an autoclave at 140°C (Method 1). Further, ZnO:graphite::2:1 nanocomposite was also fabricated in similar method by varying ZnO and graphite ratio. The nanocomposite was also fabricated directly on graphite sheets using Zn(OAc)₂·2H₂O under alkaline conditions (Method 2).

DLS data:

The dynamic light scattering (DLS) measurement confirmed that dimension of as-synthesized graphite-ZnO nanocomposite materials (~50 nm, Fig. S1, Electronic Supple-

mentary Information) are larger than the average size of graphite (~35 nm). Size distributions are narrow in all the cases.

Imaging study:

To shed light on surface morphology, Field Emission Scanning Electron Microscopy (FESEM) has been performed. Fig. S2 (Electronic Supplementary Information) represents FESEM images of graphite. The morphology is more like sheet structure consisting of flower petal shape in micrometer dimension. As we zoom in nanometer scale, uniform layered sheets can be seen (Fig. S2). The morphology of ZnO found as nanowires and nanoflowers (Fig. S3). After some modification during synthesis, ZnO nanowire transforms into nanoflowers. Fig. S3 (Electronic Supplementary Information) represents the SEM images of ZnO nanowires and nanoflowers. The width of as-synthesized ZnO baby nanowires was ~50 nm. After some synthetic modifications, the baby nanowires transformed into nanoflowers consisting of nanorods with an average width ~1 μm. The morphology of the arrayed nanowire was rod-shaped, while nanoflower was floral-shape consisting of tiny nanorods.

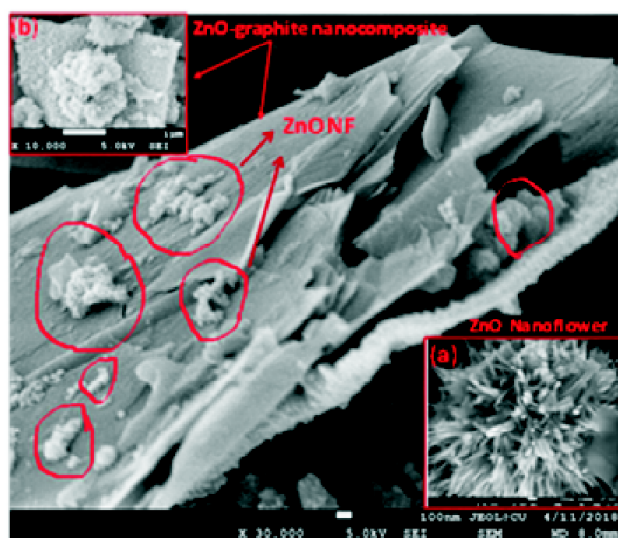


Fig. 1. FESEM images of as-synthesized ZnO-graphite nanocomposite (1:1), inset: (a) zoomed view of ZnO nanoflowers, (b) view of nanocomposites in micrometer scale.

The morphology of as-synthesized graphite:ZnO::1:1 composite looks as printed sheet-like graphite, consisting of tiny ZnO nanorods and nanoflowers embedded within graphite sheets (Fig. 1 and Fig. S4, Electronic Supplementary In-

formation). On the other hand, a morphological change was prominent in the as-synthesized graphite-ZnO nanocomposites with 2:1 ratio (Fig. S5, Electronic Supplementary Information). The morphology of ZnO composite (2:1) looks like a lump of nanoflowers grown on graphite sheets. Insertion of additional ZnO nanorods and nanoflowers in later case is responsible for this morphology change. On zooming into the nanometer scale, growth of ZnO nanoflowers on graphite sheets are clearly visible in both of the composite materials (Figs. S4, S5, Electronic Supplementary Information).

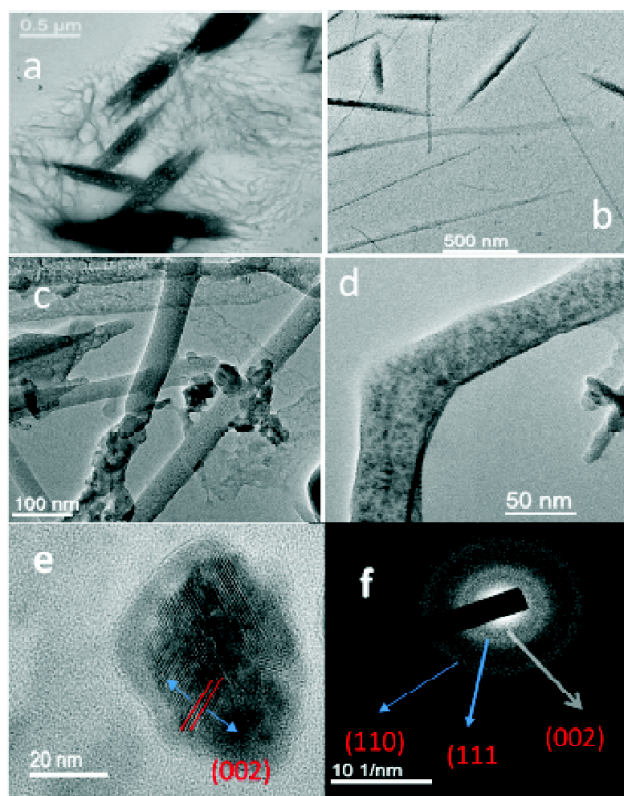


Fig. 2. TEM images of as-synthesized ZnO-graphite nanocomposite (1:1) in (a) 0.5 μm scale, (b) 500 nm scale, (c) 100 nm scale, (d) 50 nm scale, (e) HRTEM, (f) SAED pattern.

The Transmission Electron Microscopy (TEM) was undertaken to get insights of the nanomaterials such as size, distribution, and crystallinity of the synthesized materials. The TEM images (Fig. S6, Electronic Supplementary Information) of graphite reveal graphite sheet consisting uniformly distributed particles having an average size of 20 nm. The graphite-ZnO nanocomposite looks like porous sheets, which consists of ZnO nanorods filled with graphite particles (Fig.

2a,b). The average length of nanorods is $\sim 1 \mu\text{m}$ with an average width $\sim 50 \text{ nm}$ (panel c, d, Fig. 2). The HRTEM images confirm the existence of excellent lattice fringes (panel e), which suggests good crystallinity of the material, HRTEM analysis also confirms existence of graphite 002 plane (Fig. 2e). Further, the selected area electron diffraction (SAED) ring pattern (panel d) confirms polycrystallinity of the nanocomposite. SAED analysis suggests the presence of graphite 002, 110 and 111 planes. The EDS analyses (Fig. S7, Electronic Supplementary Information) confirm the existence of an enhanced amount of zinc and oxygen in the ZnO-graphite composite with ZnO:graphite::2:1, compared to the composite with ZnO:graphite::1:1.

FTIR spectroscopy:

The combined FTIR spectra of ZnO nanorods, graphite and the as-synthesized graphite:ZnO::1:1 composite are displayed in Fig. S8 (Electronic Supplementary Information). The FTIR spectrum of graphite shows characteristics of C-H stretching, whereas characteristics of Zn-O stretching, O-H stretching and bending⁶² are present in the spectrum for ZnO NPs. In the FTIR spectra of the composite, a mixture of C-H⁶³, Zn-O and O-H stretching are observed (Fig. S8). It suggests the as-synthesized graphite-ZnO as a composite materials.

X-Ray diffraction analyses:

The X-ray diffraction studies of graphite, ZnO nanoflowers and the nanocomposite (Supporting Information) were carried out in order to comprehend the crystal structure and planes of the materials. The JCPDS card analyses suggest the presence of 002 planes in graphite sample (Fig. S9, a, Electronic Supplementary Information)⁶⁴. The XRD pattern of ZnO nanowires revealed the existence of a hexagonal wurtzite structure. Further, XRD pattern of ZnO nanoflowers (NFs) exhibited characteristic peaks corresponding to 110, 002, 101, 102, 103, 112 planes (Fig. S9, b, Electronic Supplementary Information)⁶⁵. The XRD pattern for the composite nano-materials showed characteristics of graphite 002 plane, and ZnO 110, 002, and 101 planes. The disappearance of several ZnO-peaks in the nanocomposite (Fig. S9, c, Electronic Supplementary Information) might be attributed to the fact that insertion of ZnO nanoflowers within the graphite damaged the crystal planes of pure ZnO⁶⁶. Thus, the PXRD analyses suggest the as-synthesized nanomaterials are composite of ZnO and graphite.

XPS evaluation:

The X-ray photoelectron spectroscopic (XPS) analysis of nanocomposite (Fig. 3a) reveals C1s peak of binding energy 284.4 eV⁶⁷⁻⁷⁰ for carbon, which is shifted a little compared to the characteristic peak of graphite (284.09 eV). However, existence of carbon sp² hybridization is confirmed in both graphite and the composite⁶⁷⁻⁷⁰. A prominent O1s narrow peak was observed at 531.9 eV and a broad O1s peak was observed at 536.4 eV (Fig. 3b) in case of pure ZnO nanoflowers. The peak at lower binding energy 531.9 eV can be ascribed to O²⁻ ions of Zn-O bond in wurtzite structure of ZnO nanoflowers, whereas the peak at higher binding energy can be allotted to O²⁻ and O⁻ ions in the oxygen-deficient region of the as-synthesized ZnO nanoflowers⁶⁷⁻⁷⁰. The O1s peak in the composite is observed at 533.5 eV, this peak corresponds to the oxygen of Zn-O bond. This peak has also shifted in the graphite-ZnO composite compared to pure ZnO nanoflowers. However, the O1s peak signifying oxygen deficient region in ZnO disappeared, which suggests the removal of oxygen-deficiency in the composite. The doublet Zn2p₃ peaks of pure ZnO nanoflowers are lying at 1021.57 eV and 1044.65 eV, respectively (Fig. 3c), which are the spin-orbit binding energies for Zn2p_{3/2} and Zn2p_{1/2} confirming the presence of a divalent oxidation state of zinc. This is close to Zn2p binding energy in standard ZnO sample⁶⁷⁻⁷⁰. The doublet Zn2p peaks are shifted in the composite to 1024.50 eV and 1047.67 eV. All of the C1s, O1s and Zn2p peak shift may be due to insertion of ZnO-NFs inside the graphite layers in the nanocomposite. The peak shift also suggests that some sort of interaction is occurring between ZnO and graphite inside the composite, which in turn changes the electronic environment resulting in the peak shift. The combined spectra of graphite, ZnO nanoflowers, and graphite-ZnO nanocomposite are shown in Fig. S10 (Electronic Supplementary Information).

Photophysical studies:

With these characterization data in hand, the photophysical property of the graphite-ZnO nanocomposite was investigated.

UV-Vis analyses: The graphite powder-dispersed water solution showed a broad absorption spectrum with a peak at 265 nm and a hump around 350 nm (G, Fig. 4a). This obser-

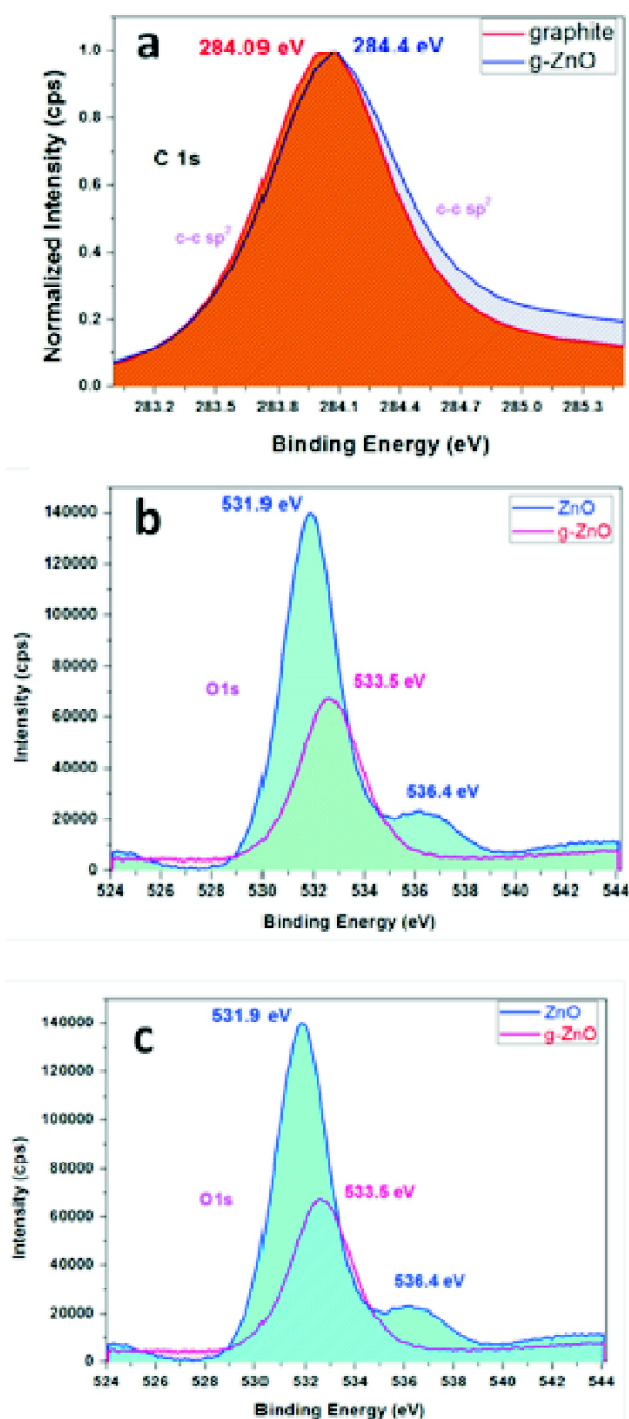


Fig. 3. Typical XPS profile: (a) C1s of graphite and graphite-ZnO nanocomposite, (b) O1s of ZnO nanoflower and graphite-ZnO nanocomposite, (c) Zn2p of ZnO nanoflower and graphite-ZnO nanocomposite.

vation is similar as reported by Theerthagiri *et al.*⁷¹ The ZnO-NPs dispersion in water displayed the absorption maxima at

375 nm, which is characteristics for ZnO NPs⁷² (Fig. S11a, Electronic Supplementary Information). The nanocomposite (G-ZnO, 1:1) exhibited two absorption peaks at 270 nm and 375 nm (Fig. 4a). These observations suggest that the nanocomposites have characteristics of both graphite and ZnO nanoflowers.

Steady state and time-resolved fluorescence spectroscopy: The aqueous dispersion of graphite powder emitted a strong fluorescence emission at a maxima 425 nm with a hump at 350 nm (Fig. S12) and ZnO-NPs showed fluorescence sharp peak at 395 nm and a broad peak ~600 nm (Fig. S11b), which is characteristics of ZnO NPs⁷². The fluorescence of ZnO NPs was measured in three different regions. We obtained almost similar type fluorescence char-

acteristics in four areas, however fluorescence intensity was different. The observation is described in Fig. S11c, ESI. Size distribution of ZnO nanoparticles dispersed in water have been recorded (Fig. S11d, ESI). Size distribution was found to be narrow. Both of these suggest moderate homogeneity of ZnO particles dispersed in water.

The fluorescence emission of as-synthesized ZnO-graphite nanocomposite (1:1) was carried out at different excitation wavelengths in a series of polar and non-polar solvents. In water, the emission maxima appeared with a bathochromic shift upon increasing excitation wavelength without significant drop off intensity in the longer wavelength region (Fig. 4c,d). The emission maxima of the composite shifted from 400 nm to 500 nm, upon excitation ranging from 340 nm to

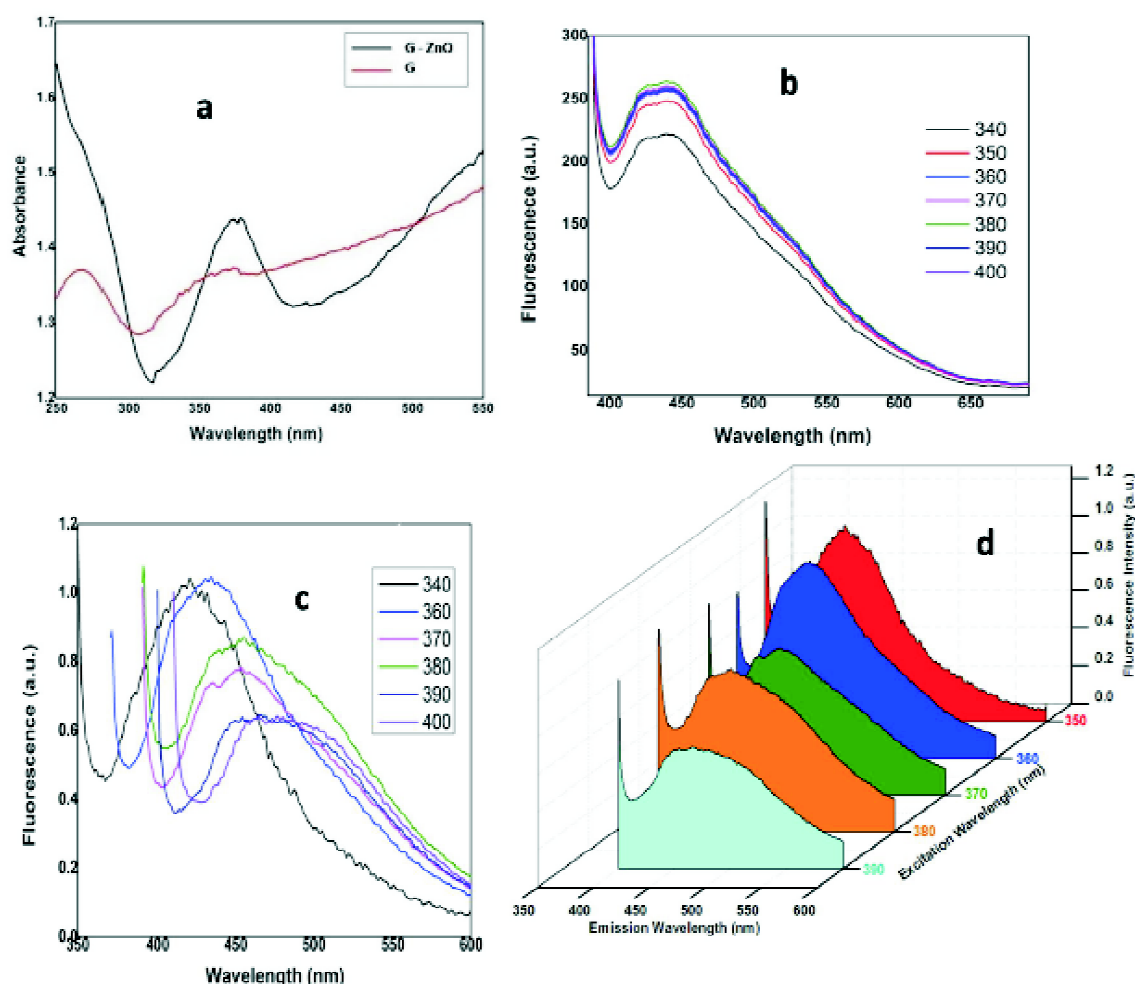


Fig. 4. (a) Absorption spectra and (b) fluorescence spectra in hexane of ZnO-graphite nanocomposite at diverse excitation wavelengths, (c) emission spectra of ZnO-graphite nanocomposite in the water at diverse excitation wavelengths, (d) 3-dimensional presentation of fluorescence emission of the graphite-ZnO composite at different excitation wavelengths.

400 nm, whereas no shift was observed in non-polar solvent hexane (Fig. 4b). The excitation-dependent emission phenomenon of the nanocomposite (g:ZnO = 1:1) was also observed in other polar and/or protic solvents such as methanol, isopropanol, DMSO, acetonitrile, and the corresponding fluorescence spectra showed lower red-shift relative to that of water (Fig. S13, Electronic Supplementary Information). However, no shift in the emission maxima was observed in non-polar solvent, hexane, benzene, and toluene using varied excitation wavelength.

Thus, the graphite-ZnO composite is displaying unprecedented excitation-dependent fluorescence characteristics of the polar solvent. The calculated fluorescence quantum yield of the as-synthesized nanocomposite is 6%. Herein, the luminescence spectra of graphite denote trap state emission, whereas the composite exhibits more of band-edge emission. The band-edge fluorescence emission of ZnO-graphite nanocomposite might be attributed to the inherent defect states of graphite, which are being removed after forming the composite with ZnO.

To get more insights of ZnO-graphite nanocomposites, ZnO:graphite::1:1 composite was synthesized following *in situ* method (Method 2), which also displayed excitation dependent fluorescence emission (Fig. 5a). The emission maxima shifted from 425 nm to 470 nm, upon excitation wavelength ranging from 300 nm to 400 nm. The shift in the emission maxima upon varying the same excitation range in the *in situ* composites (Method 2) was less than the composite synthesized in the previous approach (Method 1). However, its fluorescence intensity remains appreciable in the longer wavelength region. Since a larger shift was obtained in emission from the composite synthesized in Method 1, compared to that of composite synthesized in Method 2, further studies were performed with the composite synthesized through Method 1. The excitation dependent emission of the 1:1 composite is not dependent on polarization. The fluorescence anisotropy value remains almost constant at different excitation wavelengths for graphite-ZnO 1:1 nanocomposite (Method 1) (Fig. S13a).

Next, the fluorescence of graphite-ZnO nanocomposite with composition ZnO:graphite ratio 2:1 was investigated in order to establish the effect of graphite:zinc oxide ratio on fluorescence. Unpredictably, no shift in fluorescence maxima

was observed by changing excitation wavelength for the graphite-ZnO nanocomposite (Fig. S13b, Electronic Supplementary Information).

The excitation dependent fluorescence of carbon-based materials was extensively investigated^{41–46} to understand the reason behind this unusual emission of carbon moieties. However, the exact reason behind such a significant emission behavior is yet to be established.

Cusing *et al.*⁴¹ reported that the “giant red edge effect” is the reason behind the bathochromic shift of graphene oxide fluorescence emission upon increasing excitation wavelength. The same “giant red edge effect” might be the reason behind the unprecedented fluorescence phenomenon of our nanocomposite in water and other polar and/or protic solvents. We repeated the fluorescence measurement experiments of the composite dispersed in a series of polar solvents e.g. acetonitrile, DMSO, isopropanol and methanol and non-polar solvents such as hexane, benzene, and toluene. In all of the polar solvents, excitation dependent fluorescence emission was observed (Fig. S14), however, no shift in fluorescence emission maxima was observed with increase in excitation wavelength in case of non-polar solvents (Fig. 4b). In polar solvents such as methanol, isopropanol, water, DMSO, acetonitrile, solvent interactions may influence the unusual fluorescence phenomena. The solvent interactions within polar solvent decelerate the time scale for fluorescence from excited state level to ground state level, since a new excited state is formed by solvent interaction dynamics surrounding the composite sheets. Accordingly, the fluorescence emission maxima shifted to the longer wavelength region and the peak broadening occurred with the increase in excitation wavelength. The solvent interaction was absent in non-polar solvent (benzene and toluene) and expectantly no red shift was observed.

Gratifyingly, in contrary to the previously reported excitation-dependent emission of carbon-based materials^{41–46}, our synthesized graphite-ZnO nanocomposite exhibits the unique excitation-dependent emission in water without a noteworthy decrease in fluorescence intensity in the longer wavelength region (Figs. 4c,d, 5a). Therefore, this excitation-dependent emission of our as-synthesized graphite-ZnO nanocomposite can be extremely useful for several applications in the area of sensing, imaging, and photovoltaics.

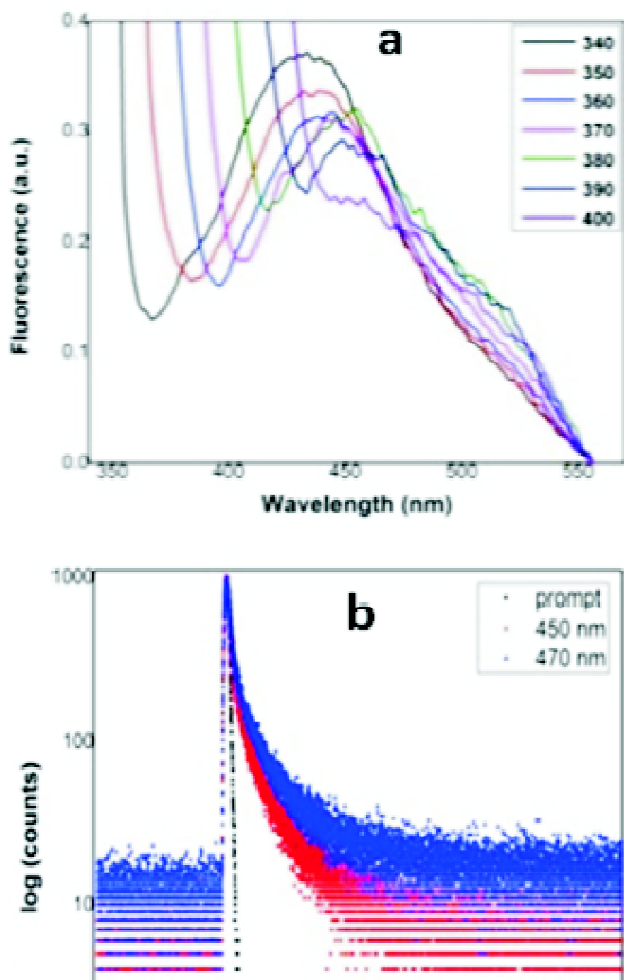


Fig. 5. (a) Fluorescence emission spectra of nanocomposite (Method 2) at different excitation wavelengths in water and (b) typical decay profile of composite in the wavelength 450 nm and 470 nm.

However, with increasing excitation wavelength towards the longer wavelength region, the full width at half maxima (FWHM) of the emission spectra enhances, and the band-edge emission leads to more trap state emission.

The time-resolved fluorescence was measured for graphite as well as the composite (Method 1) in the water at three different emission wavelengths, namely 420 nm, 440 nm and 460 nm with excitation wavelength 375 nm. The typical decay profile of graphite and the composite at emission wavelength 420 nm and 440 nm are shown in Fig. 6a,b, respectively. The decay profiles were fitted using tri-exponential fitting (Tables S1-S3, Electronic Supplementary Information),

which displayed the decay parameters at emission wavelength 420 nm, 440 nm, and 460 nm. The lifetime value was almost the same for graphite and the composite at an emission wavelength of 420 nm. However, the lifetime values were much shorter for the composite, compared to graphite at longer emission wavelengths (440 and 460 nm).

The shortened lifetime of the composite compared to graphite at longer wavelength region might be owing to the destabilized excited state caused by surrounded polar solvent interactions to the composite sheets. The typical fluorescence decay profile of the composite graphite:ZnO::1:1 (synthesized following *in situ* method i.e. Method 2) is illustrated Fig. 5b. The fluorescence decay parameters were recorded at two different emission wavelengths, e.g. 450 nm and 470 nm (Table S4, Electronic Supplementary Information). The fluorescence lifetime value of the composite synthesized *in situ* method is higher compared to both graphite and the ZnO-graphite composite synthesized in Method 1. The nanocomposite was synthesized in Method 1, where ZnO was first synthesized and then mixed with graphite. The composite was synthesized in *in situ* method (Method 2), where Zn-salt and graphite was mixed so that there is a well-mixing. It is well-known that graphite has inherent surface defects. The surface defects of graphite are being removed with addition of ZnO in the surface of the composites. The surface defects are being removed in better way in the *in situ* composite (Method 2), compared to the other one (Method 1) due to better mixing. This phenomenon is evident in the fluorescence spectra of the composites. The fluorescence spectra of *in situ* composite is narrow, which mostly signifies band edge emission (Fig. 5a). The fluorescence spectra of composite (Method 1) is comparatively broad, signifying mixture of band-edge emission and trap state emission (Fig. 4c). Thus the *in situ* composite is having lesser trap states, i.e. surface defects. so its excited state is more stabilized than the composite synthesized in other method. As a result, the excited state lifetime is greater for the *in situ* composite.

The mechanism of excitation dependent emission of our as-synthesized graphite-ZnO nanocomposite is similar to graphene oxide or other carbon based nanomaterials. However, most of the previously reported excitation dependent emission of carbon based materials suffer from the drawback of quenching their fluorescence intensity in the longer

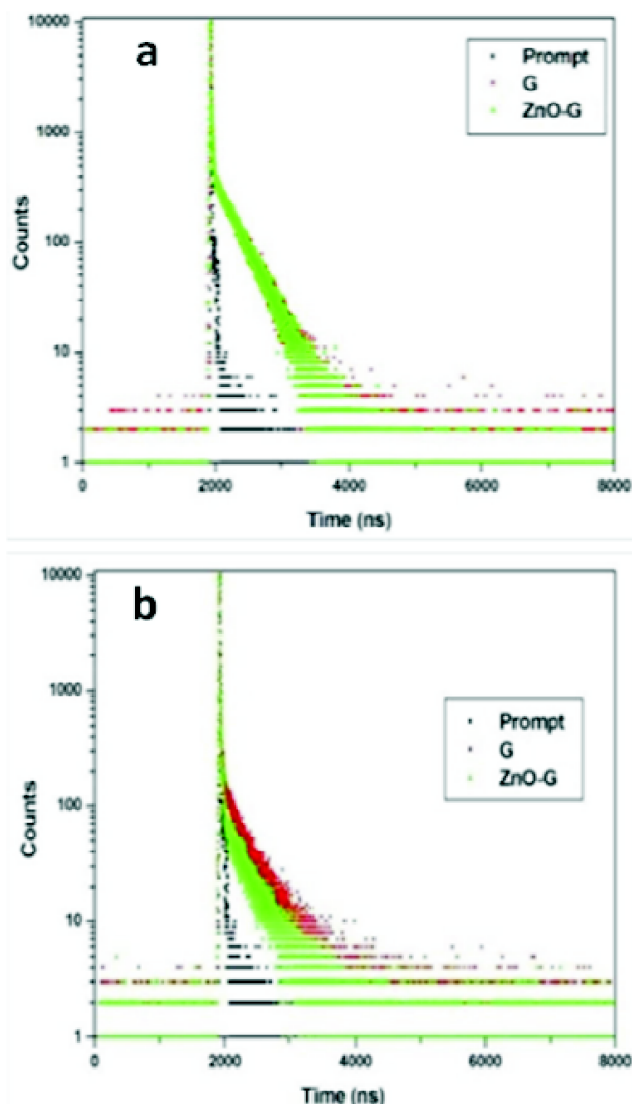


Fig. 6. Typical fluorescence decay profile of graphite and composite recorded at emission maxima: (a) 420 nm and (b) 440 nm.

wavelength region. Our as-synthesized graphite:ZnO nanocomposite 1:1 displayed significant fluorescence intensity in longer wavelength region. It is well known that carbon based nanomaterials have inherent surface defects, which can give rise to trap state emission. This trap state might be attributed to diminishing fluorescence intensity of excitation dependent fluorescence for carbon based nanomaterials in the longer wavelength region. In our case of graphite:ZnO 1:1 nanocomposite, surface defects of graphite are being removed with insertion of ZnO nanomaterials, which is evident from the fluorescence spectra of graphite only (Fig. S12,

ESI) and graphite-ZnO nanocomposite (Fig. 4c). However, comparing the FESEM images of ZnO:graphite = 1:1 (Fig. 1, S4, ESI) and 2:1 nanocomposites (Fig. S5), it is clearly seen that amount of ZnO is much more higher in case of 2:1. Therefore, in case of 1:1 composite, surface defects of graphite is being removed; whereas in case of 2:1 composite, surface defects of graphite are being removed, but additional defects are being incorporated due to presence of excess ZnO. So, new trap state is being generated in 2:1, which is evident from the PL spectra (Fig. S13). The newly created trap states in 2:1 composite probably inhibits the formation of polar solvent induced excited states, as proposed in the mechanism of excitation dependent emission. As a result, 2:1 composite does not exhibit excitation dependent emission (Fig. S13).

Implications in sensing toxic anion:

ZnO-graphene oxide nanocomposites have been very popular as chemical gas sensors^{48,58}. ZnO-graphene oxide nanocomposite has also been used as electrochemical sensor for sensing amino acids⁵⁹. However, potentials applications of this type of nanocomposites have not been explored in designing fluorescence based sensing. Here, we envision to establish the utility of the unusual excitation-dependent fluorescence property of the ZnO-graphite composite in water for fluorescence based sensing toxic analytes present in drinking water or industrial effluents. To our delight, the fluorescence intensity of the composite enhanced monotonically at an excitation wavelength 340 nm upon addition of sodium cyanide solution in the concentration range of 0.2 μM to 15 μM , the fluorescence enhancement continued upto millimolar concentration of cyanide. The fluorescence enhancement saturated in 17 mM concentration of cyanide. The observation is illustrated in Fig. 7a. The linear range for detection in our method is 0.2 μM to 15 μM , the detection limit is 0–17 mM concentration of cyanide. The World Health Organization (WHO) has quantified limit of cyanide concentration to be 1.9 mM (70 ppb)⁷⁴ in food and drinking water, as reported by Zhang *et al.*⁷⁵ and Thanayupong *et al.*⁷⁶. Thus our sensor can sense cyanide beyond the limit specified by WHO. The fluorescence enhancement was so drastic that it was even visible in the naked eye, the solution turns colorless to blue immediately. The quantum yield of the nanocomposite enhanced from 0.06 to 0.62 upon addition of 17 mM of cyanide. This observation is similar to Jeong *et al.*⁷⁷. Utilizing

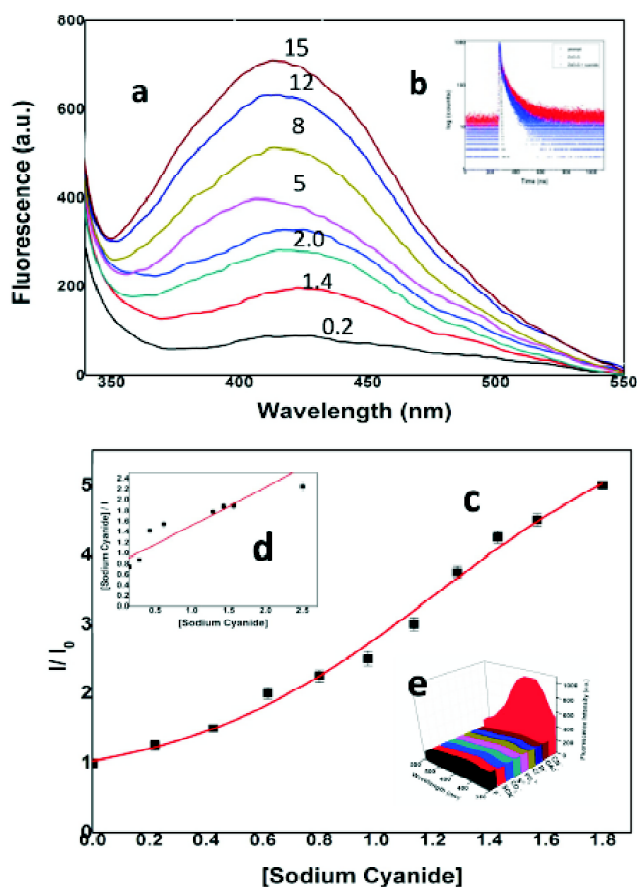


Fig. 7. (a) Fluorescence intensity enhancement of graphite-cyanide composite with addition of NaCN of conc. 0.2 μM to 15 μM ; (b) Inset: typical decay profile of composite with and without 0.15 mM NaCN; (c) plot of I/I_0 vs conc. of NaCN added; (d) inset: Langmuir binding isotherm [inset plot of C/I vs C for adsorption of NaCN on ZnO-graphite nanocomposite (1:1); (e) effect of other interfering ions similar to cyanide.

this fluorescence enhancement phenomenon, a sensor can be designed for the qualitative detection of cyanide in an easy and rapid method. Moreover, utilizing the excitation dependent-emission property of the composite, fabrication of multichannel chemical nose array based sensor^{78–81} is possible for detection of different types of environmentally and physically toxic anions similar to cyanide. Thus the unusual fluorescence of the composite has tremendous application in the arena of sensing technology.

The fluorescence of the composite was quite responsive in presence of sodium cyanide, the fluorescence enhancement followed Langmuir binding isotherm⁸² (eq. (1)) in the concentration variation range.

$$\frac{C}{I} = (1 + K_b I_{\max}) + \left(\frac{1}{I_{\max}} C \right) \quad (1)$$

where K_b is the binding constant for cyanide adsorption in the surface of the nanocomposite, I and I_{\max} represent the fluorescence intensity of the composite at a given concentration of sodium cyanide and the observed maximum fluorescence intensity of the composite respectively. Fig. 7c represents the plot of (I/I_0) vs concentration of sodium cyanide added, Fig. 7d (inset) shows the plot of (C/I) vs concentration of added cyanide. I is the fluorescence intensity of the ZnO-graphite nanocomposite at a given concentration of sodium cyanide added (C), I_0 is the initial fluorescence intensity of the composite. We checked the interference of other ions similar to cyanide (e.g. F^- , Cl^- , Br^- , SCN^- , CO_3^{2-} , S^{2-} , OAc^-) on fluorescence of as-synthesized graphite-ZnO nanocomposite, fluorescence of the nanocomposites remained unaffected in presence of aforesaid anions similar to cyanide. The phenomenon has been illustrated in Fig. 7(e). Moreover, the as-synthesized graphite-ZnO 1:1 nanocomposite was tested for determining the cyanide concentration in real water samples, corresponding results are illustrated in Table S6, ES1. Drinking water sample collected from tap and packaged mineral water samples were jagged with cyanide samples of two known concentrations (10 and 15 μM). Both of the samples were analyzed for 3 times. The CN^- concentration was determined for each sample. As shown from the table, our suggested sensing method gave reasonable analytical accuracy (<10% error) with high precision (R5D <5%)⁷⁶.

Thus, utilizing the above Langmuir binding isotherm curve, quantitative detection of toxic anion cyanide is possible by the nanocomposite in a simple, fast and non-hazardous way.

The binding constant (K_b) for the adsorption of sodium cyanide on ZnO-graphite nanocomposite was calculated from the slope/intercept value of the linear plot of C/I vs C ⁸², the numerical value of the binding constant is 2.05 M^{-1} . The small value of binding constant suggests that no new complex with covalent bonding has been formed by interaction of nanocomposite with cyanide, high value of binding constant is often associated with formation of a new complex with covalent bonding, as reported by Jeong *et al.*⁷⁷.

The drastic enhancement of fluorescence intensity of

ZnO-graphite nanocomposite with the addition of sodium cyanide might be attributed to the fact that graphite has many intrinsic defects⁷³, also ZnO nanoparticles have inherent surface defects⁸³. Consequently, ZnO-graphite nanocomposite has also several intrinsic defect states. Adsorption of sodium cyanide to the surface of the composite might help passivating the surface, which in turn augments the fluorescence intensity by removing the surface defects⁸².

The lifetime of the composite was enhanced in the presence of 15 mM Na-cyanide solution (Fig. 7a inset, Table S5, Electronic Supplementary Information). The enhancement of fluorescence intensity as well as lifetime of the composite in the presence of cyanide ion suggests that a new fluorescent species might have been formed by the interaction of ZnO-graphite composite with NaCN⁸².

The fluorescence of graphite-ZnO (ZnO:graphite ratio 2:1) also enhanced in the presence of cyanide anion in similar concentration range. However, the I/I_0 vs cyanide concentration curve for this enhancement was linear-fit (Fig. S15, Electronic Supplementary Information), whereas the I/I_0 vs cyanide concentration plot for graphite-ZnO composite (1:1) was sigmoidal fit. In both cases, pH of the composite solution enhances from 7 to 12 in the presence of cyanide ion, i.e. pH is the ideal condition for this sensor system. Our sensor acts in the similar range of pH, as reported by Dong *et al.*⁸⁴. This may be due to the fact that in both cases the sensor system is carbon based nanomaterials. Utilizing this fluorescence enhancement phenomenon, a sensor can be designed for the quantitative detection of cyanide in different samples through an easy, rapid and inexpensive method. Moreover, utilizing the excitation dependent emission property of the composite, fabrication of multichannel chemical nose array based sensor^{78–81} is possible for detection of different types of environmentally and physically toxic anions similar to cyanide. Thus, the unusual fluorescence of the composite has tremendous application in the arena of sensing science and technology.

Conclusion

In conclusion, the as-synthesized ZnO-graphite nanocomposites exhibit unique excitation-dependent emission without noteworthy drop in their fluorescence intensity in the longer wavelength region. Furthermore, the fluorescence intensity of the composite enhances significantly in the presence of micro molar cyanide anion in water. Thus,

unprecedented excitation-dependent emission coupled with the fluorescence enhancement phenomena of the nanocomposite in the presence of cyanide can pave the way for the design of multichannel array-based sensors for detection of health hazards present in drinking water, blood samples and waste effluents in a simple, inexpensive and rapid way.

Acknowledgements

Financial support from Government of India through SERB NPDF project (No. PDF/2017/000797), NPDF research fellowship to SM and SRF-CSIR to TG, and imaging facility of CRNN, CU are gratefully acknowledged.

Notes and references

1. H. W. Tseng, J. Y. Shen, T. Y. Kuo, T. S. Tu, Y. A. Chen, A. P. Demchenko and P. T. Chouhough, *Chem. Sci.*, 2016, **79**, 655.
2. Y. Zhou, G. Baryshnikov, X. Li, M. Zhu, H. Agren and L. Zhu, *Chem. Mater.*, 2018, **30**, 8008.
3. A. P. Demchenko, V. I. Tomin and P. T. Chou, *Chem. Rev.*, 2017, **117**, 13353.
4. H. Baughman, A. A. Zakhidov and W. A. de Heer, *Science*, 2002, **297**, 787.
5. A. K. Geim and K. S. Novoselov, *Nat. Mater.*, 2007, **6**, 183.
6. C. Q. Ding, A. W. Zhu and Y. Tian, *Acc. Chem. Res.*, 2014, **47**, 20.
7. L. Cao, M. J. Meziani, S. Sahu and Y. P. Sun, *Acc. Chem. Res.*, 2013, **46**, 171.
8. S. N. Baker and G. A. Baker, *Angew. Chem. Int. Ed.*, 2010, **49**, 6726.
9. H. Li, Z. Kang, Y. Liu and S. T. Lee, *J. Mater. Chem.*, 2012, **22**, 24230.
10. P. G. Luo, S. Sahu, S. T. Yang, S. K. Sonkar, J. Wang, H. Wang, G. E. LeCroy, L. Cao and Y. P. Sun, *J. Mater. Chem. B*, 2013, **1**, 2116.
11. Y. Song, S. Zhu and B. Yang, *RSC Adv.*, 2014, **4**, 27184.
12. A. F. Hebard, M. J. Rosseinsky, R. C. Haddon, D. W. Murphy, S. H. Glarum, T. T. M. Palstra, A. P. Ramirez and A. R. Kortan, *Nature*, 1991, **350**, 600.
13. Z. Gan, H. Xu and Y. Hao, *Nanoscale*, 2016, **8**, 7794.
14. Y. Wang and A. Hu, *J. Mater. Chem. C*, 2014, **2**, 6921.
15. S. Y. Lim, W. Shen and Z. Gao, *Chem. Soc. Rev.*, 2015, **44**, 362.
16. L. Bao, C. Liu, Z. L. Zhang and D. W. Pang, *Adv. Mater.*, 2015, **27**, 1663.
17. J. Liu, Y. Liu, N. Liu, Y. Han, X. Zhang, H. Huang, Y. Lifshitz, S. T. Lee, J. Zhong and Z. Kang, *Science*, 2015, **347**, 970.
18. Q. Lou, S. Qu, P. Jing, W. Ji, D. Li, J. Cao, H. Zhang, L. Liu, J. Zhao and D. Shen, *Adv. Mater.*, 2015, **27**, 1389.

19. Y. Xu, M. Wu, Y. Liu, X. Z. Feng, X. B. Yin, X. W. He and Y. K. Zhang, *Chem. Eur. J.*, 2013, **19**, 2276.
20. D. Qu, Z. Sun, M. Zheng, J. Li, Y. Zhang, G. Zhang, H. Zhao, X. Liu and Z. Xie, *Adv. Opt. Mater.*, 2015, **3**, 360.
21. J. Zhou, Y. Yang and C. Y. Zhang, *Chem. Commun.*, 2013, **49**, 8605.
22. H. Nie, M. Li, Q. Li, S. Liang, Y. Tan, L. Sheng, W. Shi and S. X. A. Zhang, *Chem. Mater.*, 2014, **26**, 3104.
23. Y. P. Sun, B. Zhou, Y. Lin, W. Wang, K. A. S. Fernando, P. Pathak, M. J. Meziani, B. A. Harruff, X. Wang, H. Wang, P. G. Luo, H. Yang, M. E. Kose, B. Chen, L. M. Veca and S. Y. Xie, *J. Am. Chem. Soc.*, 2006, **128**, 7756.
24. X. Li, Y. Liu, X. Song, H. Wang, H. Gu and H. Zeng, *Angew. Chem. Int. Ed.*, 2015, **54**, 1759.
25. V. Strauss, J. T. Margraf, C. Dolle, B. Butz, T. J. Nacken, J. Walter, W. Bauer, W. Peukert, E. Spiecker, T. Clark and D. M. Guldi, *J. Am. Chem. Soc.*, 2014, **136**, 17308.
26. L. Pan, S. Sun, A. Zhang, K. Jiang, L. Zhang, C. Dong, Q. Huang, A. Wu and H. Lin, *Adv. Mater.*, 2015, **27**, 7782.
27. H. Liu, T. Ye and C. Mao, *Angew. Chem. Int. Ed.*, 2007, **46**, 6473.
28. H. Zhang, X. Xu and H. F. Ji, *Chem. Commun.*, 2010, **46**, 1917.
29. K. M. Lee, W. Y. Cheng, C. Y. Chen, J. J. Shyue, C. C. Nieh, C. F. Chou, J. R. Lee, Y. Y. Lee, C. Y. Cheng, S. Y. Chang, T. C. Yang, M. C. Cheng and B. Y. Lin, *Nature Commun.*, 2013, **4**, 1544.
30. X. Wu, F. Tian, W. Wang, J. Chen, M. Wu and J. X. Zhao, *J. Mater. Chem. C*, 2013, **1**, 4676.
31. Y. Liu, C. Y. Liu and Z. Y. Zhang, *J. Colloid Interf. Sci.*, 2011, **356**, 416.
32. Z. Gan, S. Xiong, X. Wu, T. Xu, X. Zhu, X. Gan, J. Guo, J. Shen, L. Sun and P. K. Chu, *Adv. Opt. Mater.*, 2013, **1**, 926.
33. S. L. Hu, K. Y. Niu, J. Sun, J. Yang, N. Q. Zhao and X. W. Du, *J. Mater. Chem.*, 2009, **19**, 484.
34. Q. L. Zhao, Z. L. Zhang, B. H. Huang, J. Peng, M. Zhang and D. W. Pang, *Chem. Commun.*, 2008, 5116.
35. P. Miao, K. Han, Y. Tang, B. Wang, T. Lin and W. Cheng, *Nanoscale*, 2015, **7**, 1586.
36. A. B. Bourlinos, A. Stassinopoulos, D. Anglos, R. Zboril, M. Karakassides and E. P. Giannelis, *Small.*, 2008, **4**, 455.
37. Z. Zhu, *Nano-Micro Lett.*, 2017, **9**, 25.
38. D. Maiti, X. Tong, X. Mou and K. Yang, *Front. Pharmacol.*, 2019, **9**, 1401, 1-16.
39. R. Liu, D. Wu, S. Liu, K. Koynov, W. Knoll and Q. Li, *Angew. Chem. Int. Ed.*, 2009, **48**, 4598.
40. H. Chang and H. Wu, *Adv. Func. Mat.*, 2013, **23**, 1984.
41. S. K. Cushing, M. Li, F. Huang and N. Wu, *ACS Nano.*, 2014, **8**, 1002.
42. Z. Gan, S. Xiong, X. Wu, T. Xu, X. Zhu, X. Gan, J. Guo, J. Shen, L. Sun and P. K. Chu, *Adv. Opt. Mater.*, 2013, **1**, 926.
43. L. Zhao, X. Yu, S. Zhang, X. He, L. Li, M. Jia, M. Chang, H. Pan, J. Chen, W. Wang and J. Xu, *RSC Adv.*, 2017, **7**, 22684.
44. M. J. Krysmann, A. Kelarakis, P. Dallas and E. P. Giannelis, *J. Am. Chem. Soc.*, 2012, **134**, 747.
45. D. Pan, J. Zhang, Z. Li, C. Wu, X. Yan and M. Wu, *Chem. Commun.*, 2010, **46**, 3681.
46. A. Sharma, T. Gadly, A. Gupta, A. Ballal, S. K. Ghosh and M. Kumbhakar, *J. Phys. Chem. Lett.*, 2016, **7**, 3695.
47. M. J. S. Spencer, *Prog. Mater. Sci.*, 2012, **57**, 437.
48. V. Galstyan, E. Comini, I. Kholmanov, G. Fagliaa and G. Sberveglieri, *RSC Adv.*, 2016, **6**, 34225.
49. C. Torres-Torres, M. Trejo-Valdez, H. Sobral, P. Santiago-Jacinto, and J. A. Reyes-Esqueda, *J. Phys. Chem. C*, 2009, **113**, 13515.
50. C. Torres-Torres, J. H. Castro-Chacón, L. Castañeda, R. Rangel Rojo, R. Torres-Martínez, L. Tamayo-Rivera and A. V. Khomenko, *Opt. Express.*, 2011, **19**, 16346.
51. N. S. Hussain, P. J. Cardoso, G. Hungerford, M. J. M. Gomes, N. Ali, J. D. Santos and S. Buddhudu, *J. Nanosci. Nanotechnol.*, 2009, **9**, 3555.
52. U. Oür, Y. I. Alivov, C. Liu, A. Teke, M. A. Reshchikov, S. Doğan, V. Avrutin, S.-J. Cho and H. Morkoc, *J. Appl. Phys.*, 2005, **98**, 041301.
53. L. Castañeda, O. G. Morales-Saavedra, D. R. Acosta, A. Maldonado, M. dela and L. Olvera, *Phys. Status Solid.*, 2006, **203**, 1971.
54. H. Liang and R. G. Gordon, *J. Mater. Sci.*, 2007, **42**, 6388.
55. C. Torres-Torres, M. L. Garcýa-Cruz, L. Castañeda, R. R. Rojo, L. T.-Rivera, A. Maldonado, M. Avendaño-Alejo and R. Torres-Martínez, *J. Lumin.*, 2012, **132**, 1083.
56. V. Balasubramani, S. Sureshkumar, T. Subba Rao and T. M. Sridhar, *ACS Omega*, 2019, **4**, 9976.
57. G. Singh, A. Choudhary, D. Haranath, A. G. Joshi, N. Singh, S. Singh and R. Pasricha, *Carbon*, 2012, **50**, 385.
58. J. Hao, K. Wu, C. Wan and Y. Tang, *Talanta*, 2018, **185**, 550.
59. H. Beitollahi and F. G. Nejad, *Electroanalysis*, 2016, **28**, 2237.
60. J. N. Hasnidawani, H. N. Azlina, H. Norita, N. N. Bonnia, S. Ratim and E. S. Ali, *Procedia Chem.*, 2016, **19**, 211.
61. D. Liu, Y. Lv, M. Zhang, Y. Liu, Y. Zhu, R. Zong and Y. Zhu, *J. Mater. Chem. A*, 2014, **2**, 15377.
62. C. R. Martinez, P. Joshi, J. L. Vera, J. E. R. Vick, O. Perales, S. P. Singh, *NSTI-Nanotech.*, 2011, **3**, 420.
63. M. Bera, Chandravati, P. Gupta and P. K. Maji, *J. Nanosci. Nanotechnol.*, 2018, **18**, 902.

64. Z. Q. Li, C. J. Lu, Z. P. Xia, Y. Zhou and Z. Luo, *Carbon*, 2007, **45**, 1686.
65. A. K. Zak, R. Razali, W. H. A. Majid and M. Darroudi, *Int. J. Nanomed.*, 2011, **6**, 1399.
66. L. Zhong and K. Yun, *Int. J. Nanomed.*, 2015, **10**, 79.
67. P. Mérel, M. Tabbal, M. Chaker, S. Moisa and J. Margot, *Appl. Surf. Sci.*, 1998, **136**, 105;
68. R. Wahab, S. G. Ansari, Y. S. Kim, H. K. Seo, G. S. Kim, G. Khang and H. S. Shin, *Mater. Res. Bull.*, 2007, **42**, 1640;
69. R. Al-Gaashania, S. Radimana, A. R. Dauda, N. Tabet and Y. Al-Douri, *Ceram.*, 2013, **39**, 2283;
70. R. S. Ganesh, M. Navaneethan, G. K. Mani, S. Ponnusamy, K. Tsuchiya, C. Muthamizhchelvan, S. Kawasaki and Y. Hayakawa, *J. Alloy. Compd.*, 2017, **698**, 555.
71. J. Theerthagiri, R. Sudha, K. Premnath, P. Arunachalam, J. Madhavan and A. M. Al-Mayouf, *Int. J. Hydrogen Energy*, 2017, **42**, 13020.
72. R. Raji and K. G. Gopchandran, *J. Sci. Adv. Mater. Dev.*, 2017, **2**, 51.
73. L. Li, S. Reich and J. Robertson, *Phys. Rev. B*, 2005, **72**, 1.
74. Guidelines for Drinking-water Quality, World Health Organization, 3rd ed., 2004.
75. Y. Zhang, D. Yu and G. Feng, *RSC Adv.*, 2014, **4**, 14752.
76. E. Thanayupong, K. Suttisintong, M. Sukwattanasinittd and N. Niamnont, *New. J. Chem.*, 2017, **41**, 4058.
77. E. Jeong, S. Yoon, H. S. Lee, A. Kumara and P. S. Chae, *Dyes Pigm.*, 2019, **162**, 348.
78. S. Rana, N. D. B. Le, R. Mout, K. Saha, G. Y. Tonga, R. E. S. Bain, O. R. Miranda, C. M. Rotello and V. M. Rotello, *Nat. Nanotechnol.*, 2015, **10**, 65.
79. S. Rana, N. D. B. Le, R. Mout, B. Duncan, S. G. Elci, K. Saha and V. M. Rotello, *ACS Cent. Sci.*, 2015, **1**, 191.
80. S. Rana, S. G. Elci, R. Mout, A. K. Singla, M. Yazdani, M. Bender, A. Bajaj, K. Saha, U. H. F. Bunz, F. R. Jirik and V. M. Rotello, *J. Am. Chem. Soc.*, 2016, **138**, 4522.
81. X. Li, H. Kong, R. Mout, K. Saha, D. F. Moyano, S. M. Robinson, S. Rana, X. Zhang, M. A. Riley and V. M. Rotello, *ACS Nano.*, 2014, **8**, 12014.
82. S. Mondal, S. Ghosh, D. Ghosh and A. Saha, *J. Phys. Chem. C*, 2012, **116**, 9774.
83. M. J. S. Spencer, K. W. J. Wong and I. Yarovsky, *J. Phys. Condens. Matter.*, 2012, **24**, 1.
84. Y. Dong, R. Wang, W. Tian, Y. Chi and G. Chen, *RSC Adv.*, 2014, **4**, 3701.